



Types of structured light beams and their applications in optical cryptography: A review

Allarakha Shikder¹, Praveen Kumar², Naveen K Nishchal³ and Kehar Singh⁴

^{1,3}Department of Physics, Indian Institute of Technology Patna, Patna-801 106, Bihar, India

²Department of Physics, Indian Institute of Technology Bhilai, GEC Campus, Sejbahar, Raipur-492 015, India

⁴Optics and Photonics Center, Indian Institute of Technology Delhi, New Delhi-110 016, India

Dedicated in memory of Prof John Sheridan

Structured light beams have custom-shaped spatial amplitude, phase, and polarization distributions. Generation of various types of the structured beams is possible, depending on the spatial beam profile. Such beams have found attractive applications in science and technology owing to their unique properties resulting from inhomogeneous beam shaping. This paper reviews different types of structured light beams, with numerical simulation, and their recently emerged applications. The applications of structured beams in optical information security have been discussed and simulation results have been presented. The study would be beneficial for new researchers in this emerging area of ‘Structured light’ © Anita Publications. All rights reserved.

Keywords: Structured light beams, Vortex beams, Optical angular momentum, Optical singularity, Polarization.

1 Introduction

The laser was first operated successfully in 1960 to produce coherent light beams which are well-defined. Since 1960, lasers have occupied a prominent position in many optical technologies. Recently, research interest has been growing in light beams with complex wavefront structures [1]. Shaped light beams are often known as structured light beams [2,3]. Precise control of parameters such as wavelength, amplitude, phase, and polarization of light is crucial for the practical realization of the structured light [4]. In the present scenario, structured light has become an essential tool for many optical technologies, summarized in review articles [2,3]. Many other properties have also appeared in association with the structured beams, which are crucial for the study of optical singularities [5,6], spin-orbit interactions [7], and quantum optics [8]. The structured beams have found applications in diverse areas of optics, including optical communications [9], manipulation [10], quantum information technology, metrology [11], and microscopy [12].

Structured light beams have gained importance also because of their unique properties. Poynting suggested in 1909 that light may carry angular momentum [13]. Later, Beth [14] demonstrated the rotation of a physical object (a quarter-wave plate suspended with a thread) with circularly polarized light and showed that the angular momentum of light could result in measurable mechanical torque. In a study reported by Allen *et al* in 1992 [15], it was reported that the total angular momentum of light has both spin and an orbital component. Spin angular momentum (SAM) is associated with polarization, whereas orbital angular momentum (OAM) is associated with the helical wavefront of light [16-18]. Since then, studies on different structured beams with complex wavefront and polarization structures have gained considerable attention.

Corresponding author

e mail: nkn@iitp.ac.in (Naveen K Nishchal)

This review paper summarizes different types of structured light beams and their applications. The description of OAM carrying structured beams such as Laguerre-Gaussian (LG) beams, perfect vortex beams, hypergeometric Gaussian vortex beams, and Bessel beams have been presented, respectively in Sections 2 to 5. Other types of structured light beams without OAM, such as Airy beams, Hermite-Gaussian (HG) beams, and Ince-Gaussian (IG) beams, have also been discussed, respectively in Sections 6 to 8. Section 9 explains vectorial structured beams. Use of structured beams in optical cryptography is presented in Section 10. Section 11 presents some conclusions. Finally, Section 12 contains some remarks.

2 Laguerre-Gaussian beams

The LG modes have a helical phase profile associated with an optical vortex. An optical vortex is produced when the light with a helical wavefront rotates like a corkscrew. The electric field amplitude of LG mode, which propagates along the z -direction, can be expressed as [19],

$$E_{LGB}(x, y; l) = \sqrt{\frac{2p!}{\pi(p+|l|)!}} \frac{1}{w(z)} \left[\frac{r\sqrt{2}}{w(z)} \right]^{|l|} \exp\left[\frac{-r^2}{w^2(z)}\right] L_p^{|l|}\left(\frac{-r^2}{w^2(z)}\right) \exp\left[\frac{-ik_0 r^2 z}{2(z^2 + z_R^2)} - i\psi + il\phi\right] \quad (1)$$

where ϕ denotes the azimuth angle defined as $\phi = \tan^{-1}(y/x)$, l is the azimuthal index, and $w(z) = w(0) \sqrt{1 + (z/z_R)^2}$. Here, $w(0)$ denotes the beam waist and z_R denotes the Rayleigh range. $L_p^{|l|}$ is the associated Laguerre polynomial, p is the radial nodes of intensity profile, ψ is Gouy phase given by $\psi = (2p + |l| + 1) \tan^{-1}(z/z_R)$ while $r = \sqrt{x^2 + y^2}$. LG beam has a phase singularity along its beam axis. At the singularity, the phase is indeterminate, and the light amplitude is zero resulting in the doughnut-shaped intensity profile. OAM of the LG beams arises from the azimuthal phase dependence. Figure 1(a) shows the simulated intensity of the LG beam for $l = 1, p = 1$, and the corresponding phase profile is shown in Fig 1(b). Figure 1(c) shows the beam intensity for $l = 5, p = 3$, while Fig 1(d) shows its corresponding phase.

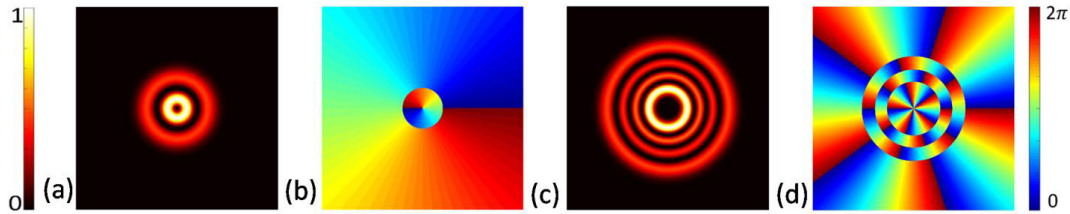


Fig 1. (a) Intensity, (b) phase profile of the LG beam for $l = 1, p = 1$; (c) intensity, and (d) phase profile for the high-order LG beam for $l = 5, p = 3$.

The LG beams have applications in diverse areas. The capability of LG beams to trap and manipulate the particles has expanded the applications of optical tweezers [20,21]. The LG beams have spiral wavefront, which can be used in optical interferometry to overcome a fundamental limitation, namely, to distinguish between elevations and depressions in a phase sample [22,23]. LG beams have brought significant innovations in quantum optics. For instance, using OAM qubits, quantum-controlled logic gates have been reported [24,25]. Using the OAM state of the LG beam, the communication system can provide an infinite bit for data encoding resulting in a cost-effective system [26]. Unbounded OAM states of LG beams have significant advantages in classical and quantum cryptographic schemes [27]. It has been reported that the OAM of a photon could be used to achieve a higher-dimensional system for quantum cryptography which results in higher information capacity and higher noise tolerance at a given security level [28]. Classical information security schemes based on OAM have also been developed to achieve a high-security holographic encryption system [29,30]. The LG beams do have astronomical applications. For instance, a vortex beam can be used to probe a weak background signal in the presence of a bright light source to detect an astronomical object [19].

3 Perfect vortex beam

Usually, the vortex beams have doughnut-shaped intensity distribution and helical phase structure. The vortex core size of these beams depends upon the corresponding topological charge (TC) value. It is the most unwanted limitation of higher-order vortex beams in several applications. To overcome this problem, perfect optical vortex beam has been proposed [31]. This beam has one circular ring shape of intensity distribution and a uniform phase gradient. At the transverse plane, the electric field profile of perfect vortex beam corresponding to topical charge l is defined [31] as

$$E_{PVB} = \exp\left(-\frac{(r-r_0)^2}{\Delta r^2}\right) \exp(il\phi) \quad (2)$$

where r_0 and Δr correspond, respectively to the radius of the toroidal part and its span. The term r can be written as $r = \sqrt{x^2 + y^2}$. The toroidal field part is independent of the TC. Figure 2(a) shows the intensity of the perfect vortex beam for $l = 3$ and the corresponding phase profile is shown in Fig 2(b). Figure 2(c) shows the intensity of the perfect vortex beam for $l = 10$ and its phase is shown in Fig 2(d).

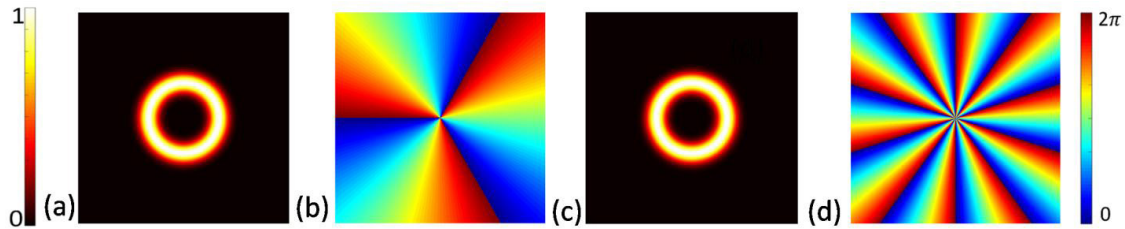


Fig 2. (a) Intensity, and (b) phase profile of perfect vortex beam for $l = 3$; (c) intensity, and (d) phase profile of perfect vortex beam for $l = 10$.

4 Hypergeometric Gaussian vortex beams

Hypergeometric Gaussian (HyG) vortex beams are another form of vortex beams that contain integer and fractional orbital momentum [32]. They are also known as the Kummer beams. Their complex amplitude is described by a degenerate HyG function in the near field. The transverse representation of the electric field of the HyG modes in the initial plane (at $z = 0$) is given [33] by,

$$E_{KB}(\rho, \phi, z = 0) = \left(\frac{\rho}{w}\right)^{m+iy} \exp\left(il\phi - \frac{\rho^2}{w^2}\right) \quad (3)$$

where (ρ, ϕ, z) is defined as the axis of cylindrical coordinates, w plays the role of beam waist corresponding to the Gaussian beam, and m is an integer. The value of γ , an integer, controls the strength of the logarithmic axicon and determines the amplitude factor's exponent. Kummer beam's profile at any distance $z > 0$ can be expressed with the help of the degenerate HyG function or Kummer function, indicating the justification of the beam name. Later in 2012, Bernardo [34] derived the beam solution for finite energy. For the case of $z = 0$, Fig 3(a) shows the intensity of the HyG beam for $m = 2, n = 2, \gamma = 2$, and the corresponding phase profile is shown in Fig 3(b). Figure 3(c) shows the intensity of the HyG beam for $m = 8, n = 6, \gamma = 4$ and the corresponding phase profile has been demonstrated in Fig 3(d).

HyG beams have excellent potential for applications in data transmission [33]. The OAM property provides multi-dimensional data transmission freedom, reducing the data transmission cost. Usually, when hyperbolic-index fibers are used for multimode data processing, it results in a greater broadening than quadratic-index fibers. But if an OAM beam is used for data transition, the infinite orthogonal eigenstate of OAM can transmit an infinite number of orthogonal modes simultaneously. Kummer beam does have OAM

property and using this beam, it is also possible to transfer data in multimode using hyperbolic-index fibers. It results in large information processing in hyperbolic-index fibers than in quadratic-index fibers.

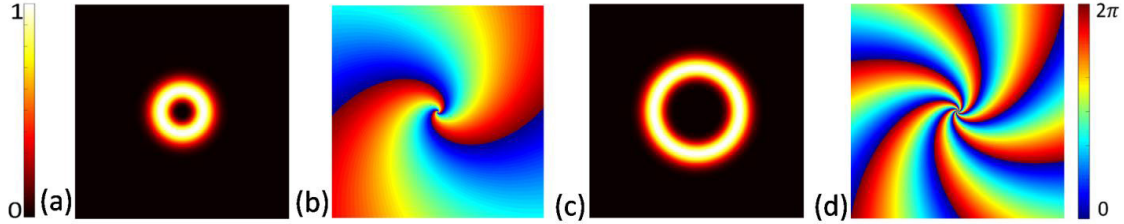


Fig 3. (a) Intensity, and (b) phase of HyG beam for $m = 2$, $n = 2$, $\gamma = 2$; (c) intensity, and (d) phase of HyG beam for $m = 8$, $n = 6$, $\gamma = 4$.

5 Bessel beams

In 1987, Durmin [35] reported Bessel beam in which, the electric field in a transverse plane is represented by the zero-order Bessel function. The expression of the electric field of a Bessel-Gaussian beam with orbital angular momentum is represented by [35],

$$E_{BB}(x, y) = J_0(\alpha\rho) e^{i(\rho^2/\omega_0^2)} e^{il\phi} \quad (4)$$

where J_0 is the zero-order Bessel function of the first kind and $\rho^2 = x^2 + y^2$. Here, l is an integer, ϕ is the azimuthal angle and ω_0 is the beam waist. The symbol α represents the transverse component of the wave vector. Figure 4(a) shows the simulated intensity of the Bessel beam for $l = 1$ and its phase is shown in Fig 4(b). Figures 4(c) and 4(d) show, respectively the intensity and phase of the Bessel beam for $l = 5$.

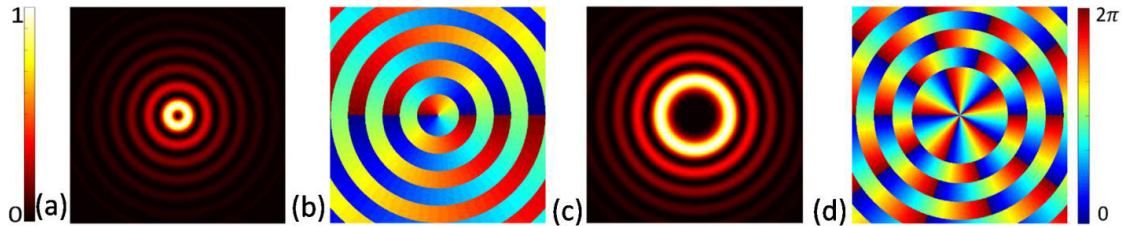


Fig 4. (a) Intensity, and (b) phase of the Bessel beam for $l = 1$; (c) intensity, and (d) phase of the Bessel beam for $l = 5$.

The intensity pattern of the Bessel beam in a transverse plane is unaltered by propagating in free-space. In addition, the Bessel beam can carry well-defined OAM. Because of these features, the Bessel beam has applications in optical trapping, material processing, and optical coherence tomography. As the Bessel beam has a narrow focus and a high gradient of optical power density, it provides an excellent flexible micromanipulation system. Researchers have also used ultrashort pulsed Bessel beams for micro-fabrication [36]. The efficiency of trapping dielectric beads in all three directions using a Bessel beam is higher than normal Gaussian beams [37]. Simultaneous trapping and rotating dielectric particles are possible using Bessel beams, as high-order Bessel beam has many ring shape intensity patterns [38,39]. Designing micro-, and nano-materials with an accuracy up to the nanoscale can be possible using Bessel beams with their non-diffractive property [40]. The elongated focal area of Gauss-Bessel beams is useful in Bragg grating engraving [41], designing microchannels [42], and photopolymerization [43].

Bessel beams have self-healing properties and can recuperate their wavefront after deformation due to any obstacle [44]. This feature raises a crucial devotion in biomedical physics, laser processing, and metrology [45]. Optical coherence tomography is an imaging process of biological tissues, cells and organs. Typical Gaussian beams are now used in endoscopic probes that do not provide a wide range of focusing

without losing resolution. However, the Bessel beams produce a much more focusing range without losing resolution than normal Gaussian beams [46-48].

6 Airy beams

The study of Airy beam was started in 1979 when Berry and Balazs [49] discovered that the motion of a particle under gravity can be expressed as an Airy function. They showed that the Airy function has a property that its probability density propagates in free-space without distortion, and with constant acceleration. It maintains its form without any outer influence, which is the most remarkable feature of the Airy packet. Airy packet is unique in propagating without change of form. The first detection of an optical Airy beam was reported by Siviloglou *et al* in 2007 [50]. It has been shown that the beam can propagate a large path without any diffraction and constantly accelerate while propagating. The main difference between the Airy beam and the Gaussian beam is that the central part of the Airy beam does not diffract but changes its position.

The Airy beams are useful in manipulation of small particles such as to govern their direction along the desired path, maybe a curve path or any bent path. This is useful in the branch of microfluidic engineering and medical applications [51]. Airy acoustical beams are capable of manipulating the cross-section trajectory of any fluid. Depending on this, acoustical tweezers have been reported like acoustical sieving and filtering [52]. The Airy beam has properties of self-bending along a parabolic curve direction, non-diffracting, self-accelerating, and self-healing, and thus they make it a potential candidate in microscopy [53], optically mediated particle clearing, particle transport, and rotation [54]. A biological cell imaging system having higher efficiency for imaging in larger abyss of the cell, can be made by Airy beam with light-sheet microscope [53,55]. It is also possible to make Airy beam having a perpetual but low-intensity profile [56]. This beam type greatly contributes to manufacturing micro and nanomaterial [55] and is also used in medical laser treatments. The mathematical expression of finite energy Airy beam can be given as [57],

$$E_{AB}(\zeta, s) = Ai \left[s_x - (\zeta/2)^2 + ia\zeta \right] + Ai \left[s_y - (\zeta/2)^2 + ib\zeta \right] * \exp \left[b(s_x + s_y) - b\zeta^2 + ib\zeta^2 - \frac{\zeta^3}{6} \frac{i\zeta(s_x + s_y)}{2} \right] \quad (5)$$

The term 'Ai' is the Airy function, $s_x = x/x_0$ and $s_y = y/y_0$ are dimensionless transverse coordinates, x and y are the transverse coordinates, x_0 and y_0 are the transverse scale parameters, $\zeta = z/kx_0^2$ is a normalized propagation distance, and $k = 2\pi/\lambda$ is the wave vector. As a result of the finite energy, this beam only maintains its non-diffractive properties over a finite distance. Figure 5(a) shows the intensity of the Airy beam for $b = 0$, and its phase is shown in Figure 5(b). Figure 5(c) shows the intensity of the Airy beam $b = 0.1$ and the corresponding phase is shown in Figure 5(d).

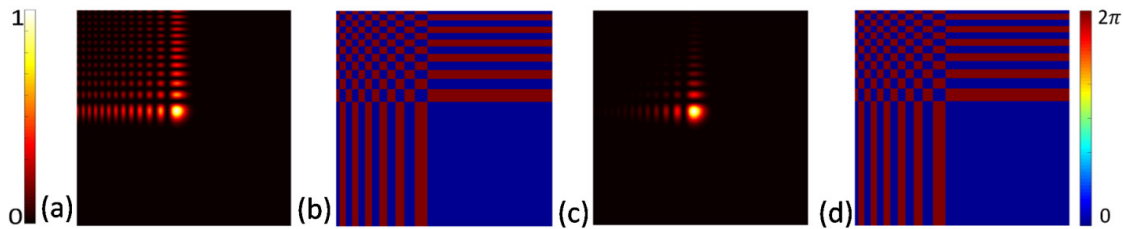


Fig 5. (a) Intensity, and (b) phase profile of Airy beam corresponding to $b = 0$; (c) intensity, and (d) phase profile of Airy beam corresponding to $b = 0.1$.

The Fourier transform of an Airy function, results in a Gaussian function with a cubic phase factor. We know that if we place an image in the focal plane of a Fourier transform lens, we obtain its Fourier

transform in the back focal plane of the lens. Therefore, to generate an Airy beam, we have to incident a Gaussian function with a cubic phase factor on the front focal plane of a Fourier transform lens, to obtain the Airy beam at the back focal plane of the lens. The generation of the Gaussian beam with a cubic phase factor can be achieved using a spatial light modulator (SLM) by displaying a cubic phase through a computer-generated hologram (CGH) on the SLM.

7 Hermite-Gaussian beams

HG beams are the solutions of the paraxial wave equation in Cartesian coordinates [58,59]. HG beams also accelerate as their maximum intensity propagates along a hyperbolic curve [57-62]. The complex amplitude of the HG beam can be expressed [59] as,

$$E_{HGB}(x, y, z) = H_n \left[\frac{\sqrt{x}}{w(z)} \right] H_m \left[\frac{\sqrt{y}}{w(z)} \right] \exp \left[\frac{r^2}{w_0^2} \right] \quad (6)$$

where H_i ($i = m, n$) is the i th order Hermite polynomial, w_0 is the beam waist, and $r = \sqrt{(x^2 + y^2)}$ is the transverse radial coordinate. Figure 6(a) shows the intensity of the HG beam for $n = 1, m = 1$ and the corresponding phase profile has been shown in Fig 6(b). Figure 6(c) shows the intensity of the HG beam for $n = 4, m = 3$ and the corresponding phase profile has been shown in Fig 6(d).

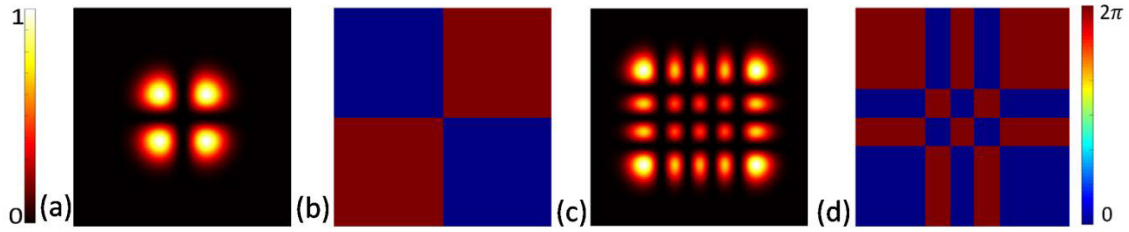


Fig 6. (a) Intensity, and (b) phase profile of HG beam corresponding to $n = 1, m = 1$; (c) intensity, and (d) phase profile of HG beam corresponding to $n = 4, m = 3$.

The HG beams have potential applications, including optical trapping, optical communications, and imaging. HG beam can also be helpful [63] in laser ablation propulsion dealing with the propagation of an object in space by using laser beam. In the case of a satellite attitude adjustment, space debris removal, and near-earth satellite launch, the importance of the laser ablation propulsion process has been increasing day-by-day. HG beams show self-healing property [64] which means it can recover its own transverse beam profile after encounter with an external influence. Due to this self-healing property, the HG beams have attracted attention in biomedical physics, laser processing, and metrology.

8 Ince-Gaussian beams

The IG beams were demonstrated by Bandres and Gutiérrez-Vega in 2004 [65]. Ince polynomials can be expressed as an IG beam's transverse structure. The IG beam has an intrinsic elliptical conformity. It is also a solution to the paraxial wave equation. The electric field of an IG beam can be given [65] as,

$$E_{IG} = D * \frac{w_0}{w(z)} C_p^m(\eta, \varepsilon) C_p^m(\eta, \varepsilon) \exp \left[\frac{-r^2}{w_0^2} \right] * \exp \left[ikz + i \frac{kr^2}{2R(z)} - i(p+1) \arctan \left(\frac{z}{z_R} \right) \right] \quad (7)$$

here w_0 is the beam width at the origin, η angular elliptic variables, z_R is the Rayleigh range and $R(z)$ is the radius of curvature of the phase front. D is the normalization constant, $C_p^m(\eta, \varepsilon)$ is even Ince polynomial of order p and degree m , where $0 \leq m \leq p$. The odd Ince polynomials can be denoted by $S_p^m(\eta, \varepsilon)$ in which the value of m is $1 \leq m \leq p$, where the indices (p) have the same parity, and ε is the elasticity parameter. The

IG beam is useful in optical trapping applications [66], bioengineering, particle manipulation, and quantum entanglement [67]. Figure 7(a) shows the intensity of the IG beam for $p = 4$, $m = 2$, and the corresponding phase profile has been shown in Fig 7(b). Figure 7(c) shows the intensity of the IG beam for $p = 6$, $m = 2$, and the corresponding phase is shown in Fig 7(d).

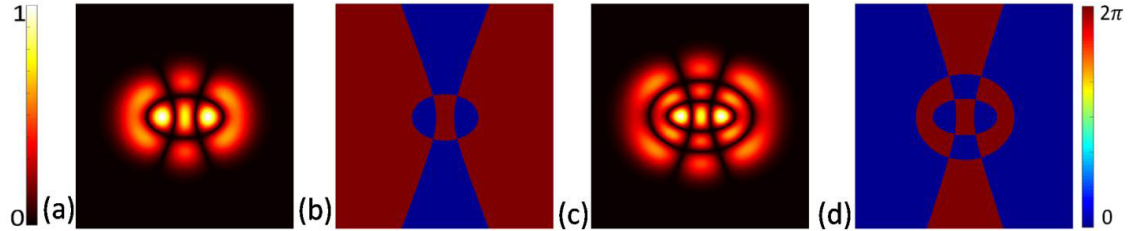


Fig 7. (a) Intensity, and (b) phase of the IG beam corresponding to $p = 4$, $m = 2$; (c) intensity, and (d) phase of IG beam corresponding to $p = 6$, $m = 2$.

9 Vectorial structured beams

The structured beams are classified as scalar and vector, depending on the polarization distribution. Structured beams with uniform polarization distribution across the transverse plane are known as the scalar beams and those with spatially-varying polarization are known as the vector beams. A special class of vector beams is a cylindrical vector (CV) beam [68]. The vector beams are the paraxial solutions of the vector wave equation and have axial symmetry in both amplitude and phase. Commonly known as CV beams, they have radial and azimuthal polarization distribution. In addition to the phase singularity, the CV beams hold V-point polarization singularity [69]. The CV beams span the equator of Poincaré sphere. Full Poincaré beam is another non-uniformly polarized beam that spans the entire surface of the Poincaré sphere. These beams hold C-point polarization singularity [69]. CV beams can be mathematically described using the Jones matrix representation. The Jones matrix representation of CV beams is given by,

$$E_{CVB} = \begin{bmatrix} E_1 \\ E_2 \end{bmatrix} = \begin{bmatrix} 1 - i & -1 - i \\ -1 - i & 1 - i \end{bmatrix} \begin{bmatrix} E_{LGB}(x, y, l_1) \\ E_{LGB}(x, y, l_2) \exp(i\delta) \end{bmatrix} \quad (8)$$

where $E_{LGB}(x, y, l_1)$ and $E_{LGB}(x, y, l_2)$ are the complex field amplitudes of LG modes given by Eq (1). Appropriate selection of the TCs l_1, l_2 and additional phase delay δ gives different orders of the polarization singularity. For beams with V-point singularity, l_1, l_2 have equal magnitudes and opposite signs, whereas for beams with C-point singularity one of the TCs, l_1, l_2 remain zero.

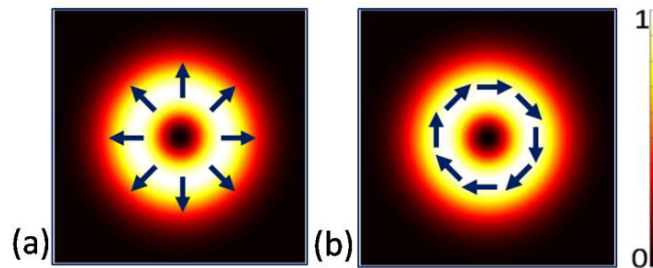


Fig 8. Intensity and polarization distributions of vectorial structured beam; (a) radially and, (b) azimuthally polarized.

For radial and azimuthal polarization distributions around V-points, the phase delay values are respectively $\delta = \pi/2$ and $3\pi/2$, whereas the TCs remain $l_1 = 1$, and $l_1, l_2 = -1$, for both cases. Figures 8(a) and

8(b) show, respectively the simulated intensity and polarization distributions of the radially and azimuthally polarized CV beams.

It has been established [69] that the radially and azimuthally polarized beams enhance trapping efficiency compared to the linearly polarized beams. It has been shown that a radially polarized beam can be used to generate a strong longitudinal field component which can be used for the engineering of tighter focusing spots [70]. Attempts are being made [71] to utilize vector beams to achieve higher resolutions and image quality. The polarization degrees of freedom of CV beams can be used as a basis to encode information and thus can be helpful in optical communication [72].

10 Optical cryptography using structured light

Optical cryptography [73-77] is a technique to encode and decode information for security purposes, using different optical properties like polarization, phase, wavelength, and optical angular momentum etc. Each of these properties of light can be utilized as the degree of freedom to encode and decode data. Larger availability of degree of freedom is desirable for any practical cryptosystem. Vortex beams have many orthogonal OAM eigenstates, a promising parameter for encoding classical or quantum information [27]. Recently, OAM holograms have been reported, in which information can be encoded in terms of an array of vortices by sampling an image in the Fourier plane and convoluting it with an OAM mode of a particular helical mode index [29]. OAM selective holograms have been proposed in which decoding is possible only with certain OAM states. Figures 9(a) shows the OAM hologram of letter 'A' and Fig 9(b) shows its reconstructed intensity distribution. Figures 9(c) shows the zoomed portion of the green box of the image shown in Fig 9(b).

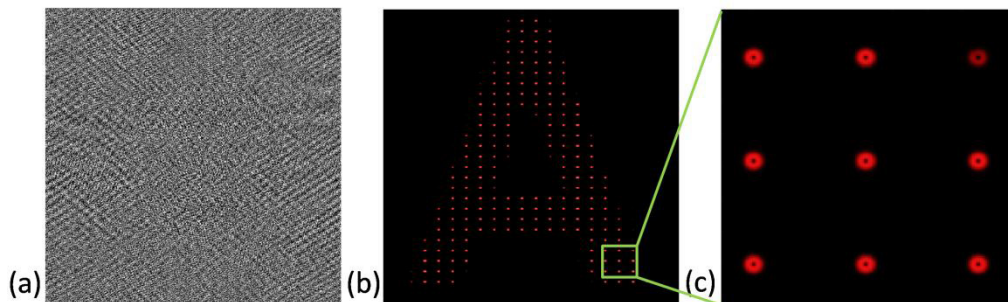


Fig 9. (a) OAM-hologram of letter 'A', (b) reconstruction of the OAM hologram, and (c) zoomed portion of the Fig 9(b).

The Vortex beams containing OAM show better stability than a normal Gaussian beam in a turbulent medium [78,79]. This property is very useful for free-space information processing applications. In this regard, a vortex lattice-based binary image encoding scheme [80] has been proposed, where the information of low-value pixels is encoded by the presence of vortex of a particular TC, and the high-value pixels are encoded by the absence of vortex. As the vortex contains dark spots at the singular phase point, it is easy to assign a threshold mean intensity value for a certain region of the lattice which returns a low-value pixel for the presence of vortex and high-value pixels for the absence of vortex at that region. This way, successful decoding of the binary image has been achieved.

Figures 10(a) and 10(b) show respectively the binary image of the numbers '2023' and the required phase distribution for encoding the data into the light beam. Figure 10(c) shows the intensity distribution of data encoded vortex lattice. This data-encoded light beam has been encrypted by modulating the phase of the light beam with an array of vortices of random TC acting as the encryption key. The phase distribution of the encryption key is shown in Fig 10(d). Figures 10(e) and 10(f) show, respectively the intensity distributions of

the encrypted beam and the encrypted image. This encrypted image is a processed image developed from the intensity distribution of the encrypted beam according to the above-mentioned way of mean intensity value measurement at the target region. **Figure 10(g)** shows the decryption key's phase distribution, which is just the conjugate of the encryption key. The successful decryption of the encoded information has been done when the encoded light beam passes through the decryption key. **Figure 10(h)** and **10(i)** show, respectively the intensity distributions of the decrypted light beam and the decrypted binary image.

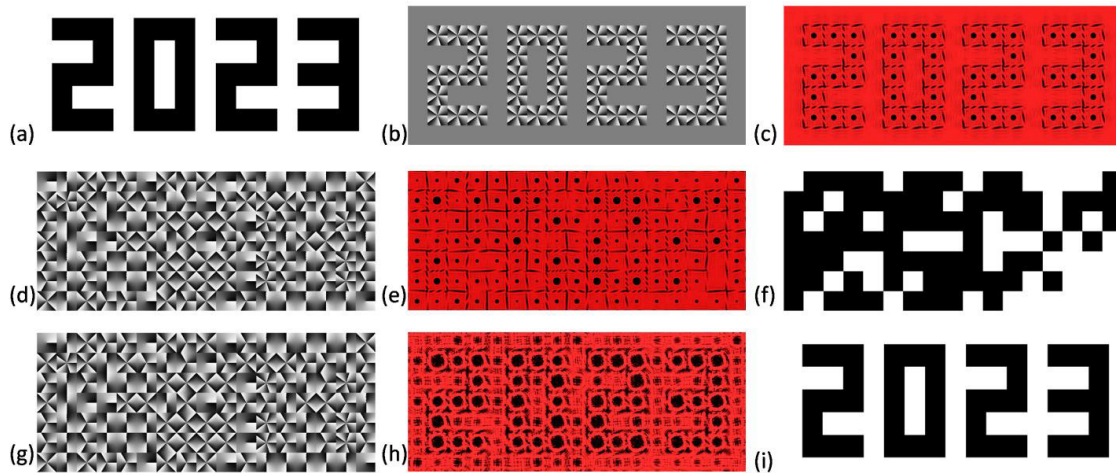


Fig 10. (a) Phase of encoded light beam containing the binary image of numbers '2023', (b) intensity distribution of the data encoded light beam, (c) processed image from the intensity distribution of the data encoded light beam, (d) phase distribution of the encryption key, (e) intensity distribution of the encrypted light beam, (f) processed image from the intensity distribution of the encrypted light beam, (g) phase distribution of the decryption key, (h) intensity distribution of the encrypted light beam, and (i) processed image from the intensity distribution of the decrypted light beam.

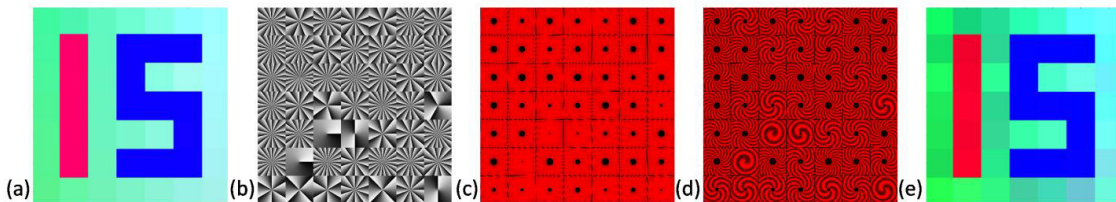


Fig 11. (a) Color image, and (b) phase distribution of the encrypted light beam; (c) intensity distribution of the encrypted light beam, (d) interference between the encrypted light beam and spherical beam, and (e) decrypted color image.

Recently, a Gerchberg-Saxton algorithm-based color image encryption system has been reported [81] where the output phase information corresponding to the color image is mapped to an array of integer numbers followed by an additional random number distribution used as the encryption key. This array of integer numbers has been encoded into the light beam in the form of an array of vortices corresponding to the TC, the same as those numbers. **Figure 11(a)**, **11(b)**, and **11(c)** show, respectively the color image of the number '15' to be encoded, the phase distribution of the encrypted beam, and the intensity distribution of the encrypted beam. The decryption of the information is achieved at the receiver end by measuring the TCs of the array of vortices and using the decryption key. The TCs of the vortices has been measured using interferometry [82-87]. **Figure 11(d)** shows the interference pattern between the encrypted and spherical beams. The TCs of the array of vortices can be easily measured by counting the number of petals of the fringes and the sign by observing the rotation direction of the fringes. Thus,

one can easily get the information of the encrypted array of numbers by observing this interference fringe and easily decrypt the information using the decryption key. Figure 11(e) shows the decrypted image.

Furthermore, several image encryption schemes [88-91] using arbitrary vector beams have been reported. Arbitrary vector beams have non-uniform polarization distribution across their transverse plane and have been found suitable for image encoding. Schemes based on three-dimensional polarization, geometric phase, and vortex spatial filters [92-94] have been suggested. Encryption schemes using vector beams are also preferred because of their simple optical implementation and pure intensity measurement-based decoding [95-98]. The polarization degrees of freedom of vector vortex beams that carry polarization singularity has also been utilized for information encoding [77,99,100]. The non-separability of vector beams can be used to encode information for optical communication applications [101,90]. These works demonstrate the expanding applications of structured light beams in information security.

11 Conclusions

This paper reviews the property and applications of some important structured light beams. Most of the beams contain important properties like OAM, self-healing, very narrow focus, highly gradient beam profile, and self-accelerating, etc. Structured beams have applications in diverse branches of science and technology including biomedical, communications, and quantum systems. Although a number of structured light beams and their applications have been reported, some challenges are still present in this field; like beam-profile manipulation in three-dimension or discovering new applications that can be realized using structured light. The use of structured beams in optical information security has been demonstrated through numerical simulations.

12 Some Closing Remarks

The subject of 'structured light beams' has become so vast that the present review is unable do full justice to the subject. We feel that within the space available to us, we are constrained to discuss only some aspects of the subject and apologize to the authors whose work has not been cited. An article by Kolomiets [102] gives an excellent summary of the publications by Kotlyar and his coworkers who have made significant contributions to the subject. The book by Kotlyar, Kovalev, and Profirev [103] contains a plethora of information on various types of the structured light beams. A more recent book by Kotlyar, Kovalev, and Nalimov [104], includes an authoritative account of some more recent advances on the subject. Books by Senthilkumaran [105], Gbur [106], and Rosales-Guzman and Forbes [107] also need to be mentioned.

Optical vortices have also been used as radial Hilbert filters [108-117] in cryptosystems using various transforms. A few more recent papers [118-122] pertinent to the subject may also be noted. Optical vortices have also been used in some other recent investigations [123,124]. More recently in 2023, fractional vortex speckle patterns have been employed in a cryptosystem [125].

Acknowledgments

The authors acknowledge the funding from the Scientific and Engineering Research Board, Department of Science and Technology, Govt. of India, under Grant No. CRG/2021/001763. A. Shikder wishes to acknowledge the financial support from Prime Minister's Research Fellowship, Government of India (ID-2701807).

References

1. Forbes A, Structured light from lasers, *Laser Photon Rev*, 13(2019)1970043; doi.org/10.1002/lpor.201900140.
2. Rubinsztein-Dunlop H, Forbes A, Berry M V, Dennis M R, Andrews D L, Mansuripur M, Denz C, Alpmann C, Banzer P, Bauer T, Karimi E, Marrucci L, Padgett M, Ritsch-Marte M, Litchinitser N M, Bigelow N P, Rosales-

- Guzmán C, Belmonte A, Torres J P, Neely T W, Baker M, Gordon R, Stilgoe A B, Romero J, White A G, Fickler R, Willner A E, Xie G, McMorran B, Weiner A M, Roadmap on structured light, *J Opt*, 19(2017)013001; 10.1088/2040-8978/19/1/013001.
3. Forbes A, Structured light: tailored for purpose, *Opt Photon News*, 31(2020)24–31.
 4. Kumar P, Nishchal N K, Formation of singular light fields using phase calibrated spatial light modulator, *Opt Lasers Eng*, 146(2021)106720; doi.org/10.1016/j.optlaseng.2021.106720.
 5. Dennis M R, O'holleran K, Padgett M J, Singular optics: optical vortices and polarization singularities, *Progr Opt*, 53(2009)293–363.
 6. Allen L, Barnett S M, Padgett M J, (Eds), *Optical Angular Momentum*, (CRC Press), 2003.
 7. Marrucci L, Manzo C, Paparo D, Optical spin-to-orbital angular momentum conversion in inhomogeneous anisotropic media, *Phys Rev Lett*, 96(2006)163905; doi.org/10.1103/PhysRevLett.96.163905.
 8. Molina-Terriza G, Torres J P, Torner L, Twisted photons, *Nat Phys*, 3(2007)305–310.
 9. Wang J, Advances in communications using optical vortices, *Photon Res*, 4(2016)B14–B28.
 10. Dholakia K, Čížmár T, Shaping the future of manipulation, *Nat Photon*, 5(2011)335–342.
 11. Rosales-Guzmán C, Hermosa N, Belmonte A, Torres J P, Experimental detection of transverse particle movement with structured light, *Sci Rep*, 3(2013)2815; doi.org/10.1038/srep02815.
 12. Fürhapter S, Jesacher A, Bernet S, Ritsch-Marte M, Spiral phase contrast imaging in microscopy, *Opt Express*, 13(2005)689–694.
 13. Poynting J H, The wave motion of a revolving shaft, and a suggestion as to the angular momentum in a beam of circularly polarised light, *Proc R Soc London A*, 82(1909)560–567.
 14. Beth R A, Mechanical detection and measurement of the angular momentum of light, *Phys Rev*, 50(1936)115–125.
 15. Allen L, Beijersbergen M W, Spreeuw R J C, Woerdman J P, Orbital angular momentum of light and the transformation of Laguerre-Gaussian laser modes, *Phys Rev A*, 45(1992)8185–8189.
 16. Nye J F, Berry M V, Dislocations in wave trains, *Proc R Soc London A*, 336(1974)165–190.
 17. Franke-Arnold S, Allen L, Padgett M J L, Reviews P, Advances in optical angular momentum, *Laser Photon Rev*, 2(2008)299–313.
 18. Barnett S M, Babiker M, Padgett M J, Optical orbital angular momentum, *Philos Trans R Soc A*, 375(2017)20150444; doi.org/10.1098/rsta.2015.0444.
 19. Yao A M, Padgett M J, Orbital angular momentum: origins, behavior and applications, *Adv Opt Photon*, 3(2011)161–204.
 20. He H, Friese M E J, Heckenberg N R, Rubinsztein-Dunlop H, Direct observation of transfer of angular momentum to absorptive particles from a laser beam with a phase singularity, *Phys Rev Lett*, 75(1995)826–829.
 21. Rosales-Guzmán C, Ndagano B, Forbes A, A review of complex vector light fields and their applications, *J Opt*, 20(2018)123001; doi. 10.1088/2040-8986/aaeb7d.
 22. Fürhapter S, Jesacher A, Bernet S, Ritsch-Marte M, Spiral interferometry, *Opt Lett*, 30(2005)1953–1955.
 23. Ritsch-Marte M, Orbital angular momentum light in microscopy, *Phil Trans R Soc A*, 375(2017)20150437; doi.org/10.1098/rsta.2015.0437.
 24. Chanu S R, Natarajan V, Narrowing of resonances in electromagnetically induced transparency and absorption using a Laguerre-Gaussian control beam, *Opt Commun*, 295(2013)150–154.
 25. Anupriya J, Ram N, Pattabiraman M, Hanle electromagnetically induced transparency and absorption resonances with a Laguerre-Gaussian beam, *Phys Rev A*, 81(2010)043804; doi.org/10.1103/PhysRevA.81.043804.
 26. Singh M, Atieh A, Grover A, Barukab O, Performance analysis of 40 Gb/s free space optics transmission based on orbital angular momentum multiplexed beams, *Alex Eng J*, 61(2022)5203–5212.
 27. Gröblacher S, Jennewein T, Vaziri A, Weihs G, Zeilinger A, Experimental quantum cryptography with qutrits, *New J Phys*, 8(2006)75; 10.1088/1367-2630/8/5/075.
 28. Mirhosseini M, Magaña-Loaiza O S, O'Sullivan M N, Rodenburg B, Malik M, Lavery M P J, Padgett M J, Gauthier D J, Boyd R W, High-dimensional quantum cryptography with twisted light, *New J Phys*, 17(2015)033033; doi.10.1088/1367-2630/17/3/033033.

29. Fang X, Ren H, Gu M, Orbital angular momentum holography for high-security encryption, *Nat Photon*, 14(2020)102–108.
30. Ruffato G, Rossi R, Massari M, Mafakheri E, Capaldo P, Romanato F, Design, fabrication and characterization of computer generated holograms for anti-counterfeiting applications using OAM beams as light decoders, *Sci Rep*, 7(2017)18011; doi.org/10.1038/s41598-017-18147-7.
31. Ostrovsky A S, Rickenstorff-Parrao C, Arrizón V, Generation of the “perfect” optical vortex using a liquid-crystal spatial light modulator, *Opt Lett*, 38(2013)534–536.
32. Kotlyar V V, Kovalev A A, Topological charge of asymmetric optical vortices, *Opt Express*, 28(2020)20449–20460.
33. Kotlyar V V, Kovalev A A, Family of hypergeometric laser beams, *J Opt Soc Am A*, 25(2008)262–270.
34. Bernardo B D L, Moraes F, Data transmission by hypergeometric modes through a hyperbolic-index medium, *Opt Express*, 19(2011)11264–11270.
35. Durnin J, Exact solutions for nondiffracting beams, I. The scalar theory, *J Opt Soc Am A*, 4(1987)651–654.
36. Amako J, Sawaki D, Fujii E, Microstructuring transparent materials by use of nondiffracting ultrashort pulse beams generated by diffractive optics, *J Opt Soc Am B*, 20(2003)2562–2568.
37. Ayala Y A, Arzola A V, Volke-Sepúlveda K, Comparative study of optical levitation traps: focused Bessel beam versus Gaussian beams, *J Opt Soc Am B*, 33(2016)1060–1067.
38. Volke-Sepúlveda K, Garcés-Chávez V, Chávez-Cerda S, Arlt J, Dholakia K, Orbital angular momentum of a high-order Bessel light beam, *J Opt B: Quantum Semiclass Opt*, 4(2002)S82; 10.1088/1464-4266/4/2/373.
39. Volke-Sepúlveda K, Chávez-Cerda S, Garcés-Chávez V, Dholakia K, Three-dimensional optical forces and transfer of orbital angular momentum from multiringed light beams to spherical microparticles, *J Opt Soc Am B*, 21(2004)1749–1757.
40. Chu X, Sun Q, Wang J, Lü P, Xie W, Xu X, Generating a Bessel-Gaussian beam for the application in optical engineering, *Sci Rep*, 5(2016)18665; doi.org/10.1038/srep18665.
41. Mikutis M, Kudrius T, Šlekys G, Paipulas D, Juodkazis S, High 90% efficiency Bragg gratings formed in fused silica by femtosecond Gauss-Bessel laser beams, *Opt Mater Express*, 3(2013)1862–1871.
42. Bhuyan M K, Courvoisier F, Lacourt P A, Jacquot M, Furfaro L, Withford M J, Dudley J M, High aspect ratio taper-free microchannel fabrication using femtosecond Bessel beams, *Opt Express*, 18(2010)566–574.
43. Yang L, El-Tamer A, Hinze U, Li J, Hu Y, Huang W, Chu J, Chichkov B N, Two-photon polymerization of cylinder microstructures by femtosecond Bessel beams, *Appl Phys Lett*, 105(2014)041110; doi.org/10.1063/1.4891841.
44. Li S, Wang J, Adaptive free-space optical communications through turbulence using self-healing Bessel beams, *Sci Rep*, 7(2017)43233; doi.org/10.1038/srep43233.
45. Bouchal Z, Nondiffracting optical beams: physical properties, experiments, and applications, *Czechoslovak J Phys*, 53(2003)537–578.
46. Lorensen D, Singe C C, Curatolo A, Sampson D D, Energy-efficient low-Fresnel-number Bessel beams and their application in optical coherence tomography, *Opt Lett*, 39(2014)548–551.
47. Yi L, Sun L, Ding W, Multifocal spectral-domain optical coherence tomography based on Bessel beam for extended imaging depth, *J Biomed Opt*, 22(2017)106016; doi.org/10.1117/1.JBO.22.10.106016.
48. Yin B, Hyun C, Gardecki J A, Tearney G J, Extended depth of focus for coherence-based cellular imaging, *Optica*, 4(2017)959–965.
49. Berry M V, Balazs N L, Nonspreading wave packets, *Am J Phys* 47(1979)264–267.
50. Siviloglou G A, Broky J, Dogariu A, Christodoulides D N, Observation of accelerating Airy beams, *Phys Rev Lett*, 99(2007)213901; doi.org/10.1103/PhysRevLett.99.213901.
51. Lu W, Chen J, Lin Z, Liu S, Driving a dielectric cylindrical particle with a one-dimensional Airy beam: a rigorous full wave solution, *Prog Electromagn Res*, 115(2011)409–422.
52. Mitri F G, Airy acoustical-sheet spinner tweezers, *J Appl Phys*, 120(2016)104901; doi.org/10.1063/1.4962397.
53. Vettenburg T, Dalgarno H I C, Nylk J, Coll-Lladó C, Ferrier D E K, Čižmár T, Gunn-Moore F J, Dholakia K, Light-sheet microscopy using an Airy beam, *Nat Methods*, 11(2014)541–544.
54. Baumgartl J, Mazilu M, Dholakia K, Optically mediated particle clearing using Airy wavepackets, *Nat Photon*, 2(2008)675–678.

55. Piksarv P, Marti P D, Le T, Unterhuber A, Forbes L H, Andrews M R, Stingl A, Drexler W, Andersen P E, Dholakia K, Integrated single- and two-photon light sheet microscopy using accelerating beams, *Sci Rep*, 7(2017)1435; doi.org/10.1038/s41598-017-01543-4.
56. Efremidis N K, Christodoulides D N, Abruptly autofocusing waves, *Opt Lett*, 35(2010)4045–4047.
57. Siviloglou G A, Christodoulides D N, Accelerating finite energy Airy beams, *Opt Lett*, 32(2007)979–981.
58. Kogelnik H, Li T, Laser beams and resonators, *Appl Opt*, 5(1966)1550–1567.
59. Aguirre-Olivas D, Mellado-Villaseñor G, Sánchez-de-la-Llave D, Arrizón V, Efficient generation of Hermite-Gauss and Ince-Gauss beams through kinoform phase elements, *Appl Opt*, 54(2015)8444–8452.
60. Kotlyar V V, Kovalev A A, Soifer V A, Transformation of decelerating laser beams into accelerating ones, *J Opt*, 16(2014)085701; doi. 10.1088/2040-8978/16/8/085701.
61. Huang C, Lu H, Accelerating propagation properties of misplaced Hermite-Gaussian beams, *J Opt Soc Am A* 31(2014)1762–1765.
62. Huang C, Li H, Wu J, Yan Y, Hyperbolic accelerating beams and their relation with Hermite-Gaussian beams, *J Opt Soc Am A*, 35(2018)262–266.
63. Fan X, Ji X, Wang H, Deng Y, Zhang H, Self-focusing effect on the beam quality of Hermite-Gaussian beams propagating upwards through the inhomogeneous atmosphere, *J Opt Soc Am A*, 38(2021)168–173.
64. Xu Z, Liu X, Chen Y, Wang F, Liu L, Monfared Y E, Ponomarenko S A, Cai Y, Liang C, Self-healing properties of Hermite-Gaussian correlated Schell-model beams, *Opt Express*, 28(2020)2828–2837.
65. Bandres M A, Gutiérrez-Vega J C, Ince-Gaussian beams, *Opt Lett*, 29(2004)144–146.
66. Woerdemann M, Alpmann C, Denz C, Optical assembly of microparticles into highly ordered structures using Ince-Gaussian beams, *Appl Phys Lett*, 98(2011)111101; doi.org/10.1063/1.3561770.
67. Wang M-Y, Tang J, Wang H-J, Ming Y, Zhang Y, Cui G-X, Lu Y-Q, Generation of second-harmonic Ince-Gaussian beams, *Appl Phys Lett*, 113(2018)081105; doi.org/10.1063/1.5041986.
68. Zhan Q, Cylindrical vector beams: from mathematical concepts to applications, *Adv Opt Photon*, 1(2009)1–57.
69. Kumar P, Pal S K, Nishchal N K, Senthilkumaran P, Non-interferometric technique to realize vector beams embedded with polarization singularities, *J Opt Soc Am A*, 37(2020)1043–1052.
70. Roxworthy B J, Toussaint K C, Optical trapping with π -phase cylindrical vector beams, *New J Phys*, 12(2010)073012; doi.10.1088/1367-2630/12/7/073012.
71. Dorn R, Quabis S, Leuchs G, Sharper focus for a radially polarized light beam, *Phys Rev Lett*, 91(2003)233901; doi.org/10.1103/PhysRevLett.91.233901.
72. Ram B S B, Senthilkumaran P, Sharma A, Polarization-based spatial filtering for directional and nondirectional edge enhancement using an S-waveplate, *Appl Opt*, 56(2017)3171–3178.
73. Kumar P, Kumar A, Joseph J, Singh K, Impulse attack free double-random-phase encryption scheme with randomized lens-phase functions, *Opt Lett*, 34(2009)331–333.
74. Nishchal N K, *Optical Cryptosystems*, (IoP Publs, Bristol, UK), 2019.
75. Unnikrishnan G, Joseph J, Singh K, Optical encryption by double-random phase encoding in the fractional Fourier domain, *Opt Lett*, 25(2000)887–889.
76. Chen W, Javidi B, Chen X, Advances in optical security systems, *Adv Opt Photon*, 6(2014)120–155.
77. Kumar P, Fatima A, Nishchal N K, Arbitrary vector beam encoding using single modulation for information security applications, *IEEE Photon Technol Lett*, 33(2021)243–246.
78. Vaity P, Singh R P, Self-healing property of optical ring lattice, *Opt Lett*, 36(2011)2994–2996.
79. Khare K, Lochab P, Senthilkumaran P, Orbital Angular Momentum States of Light: Propagation through Atmospheric Turbulence, (IoP Publs, Bristol, UK), 2020.
80. Shikder A, Kumar P, Nishchal N K, Image encryption by structured phase encoding and its effectiveness in turbulent medium, *IEEE Photon Technol Lett*, 35(2023)128–131.
81. Kumar P, Nishchal N K, AlFalou A, Controllable optical vortex array for image encoding, *IEEE Photon Technol Lett*, 34(2022)521–524.

82. Shikder A, Nishchal N K, Measurement of the fractional topological charge of an optical vortex beam through interference fringe dislocation, *Appl Opt*, 62 (2023)D58–D67.
83. Kumar P, Nishchal N K, Modified Mach-Zehnder interferometer for determining the high-order topological charge of Laguerre-Gaussian vortex beams, *J Opt Soc Am A*, 36(2019)1447–1455.
84. Kumar P, Nishchal N K, Self-referenced spiral interferogram using modified lateral shearing Mach-Zehnder interferometer, *Appl Opt*, 58(2019)6827–6833.
85. Kumar P, Nishchal N K, Self-referenced interference of laterally displaced vortex beams for topological charge determination, *Opt Commun*, 459(2020)125000; doi.org/10.1016/j.optcom.2019.125000.
86. Kumar P, Nishchal N K, Singh K, Role of self-referenced interferometry in measuring the orbital angular momentum of optical vortices: A review, *Asian J Phys* 29(2020)835–852.
87. Pachava S, Dharmavarapu R, Vijayakumar A, Jayakumar S, Manthalkar, Dixit A, Viswanathan N K, Srinivasan B, Bhattacharya S, Generation and decomposition of scalar and vector modes carrying orbital angular momentum: a review, *Opt Eng*, 59(2020)041205–041205.
88. AlFalou A, Brosseau C, Dual encryption scheme of images using polarized light, *Opt Lett*, 35(2010)2185–2187.
89. Rajput S K, Nishchal N K, Image encryption using polarized light encoding and amplitude and phase truncation in the Fresnel domain, *Appl Opt*, 52(2013)4343–4352.
90. Maluenda D, Carnicer A, Martínez-Herrero R, Juvells I, Javidi B, Optical encryption using photon-counting polarimetric imaging, *Opt Express*, 23(2015)655–666.
91. Carnicer A, Juvells I, Javidi B, Martínez-Herrero R, Optical encryption in the axial domain using beams with arbitrary polarization, *Opt Lasers Eng*, 89(2017)145–149.
92. Li X, Lan T-H, Tien C-H, Gu M, Three-dimensional orientation-unlimited polarization encryption by a single optically configured vectorial beam, *Nat Commun*, 3(2012)998; doi.org/10.1038/ncomms2006.
93. Lin C, Shen X, Hua B, Wang Z, Three-dimensional polarization marked multiple-QR code encryption by optimizing a single vectorial beam, *Opt Commun*, 352(2015)25–32.
94. Kotlyar V V, Effect of aberration on the focusing of optical vortices and the use of vortex spatial filters in cryptography, *Asian J Phys* 30(2021)955–964.
95. Fatima A, Nishchal N K, Optical image security using Stokes polarimetry of spatially variant polarized beam, *Opt Commun*, 417(2018)30–36.
96. Wang Q, Xiong D, Al Falou A, Brosseau C, Optical image authentication using spatially variant polarized beam and sparse phase sampling method, *Opt Lasers Eng*, 124(2020)105828; doi.org/10.1016/j.optlaseng.2019.105828.
97. Nishchal N K, Use of vector beam in image encryption; A review, *Asian J Phys* 30(2021)1007–1012.
98. Kumar P, Nishchal N K, Realizing singular beams through dual-phase modulation, *Asian J Phys* 30(2021)1355–1364.
99. Zhao Y, Wang J, High-base vector beam encoding/decoding for visible-light communications, *Opt Lett*, 40(2015)4843–4846.
100. Xian M, Xu Y, Ouyang X, Cao Y, Lan S, Li X, Segmented cylindrical vector beams for massively-encoded optical data storage, *Sci Bull*, 65(2020)2072–2079.
101. Milione G, Nguyen T A, Leach J, Nolan D A, Alfano R R, Using the nonseparability of vector beams to encode information for optical communication, *Opt Lett*, 40(2015)4887–4890.
102. Kolomiets E I, For the Jubilee of Professor Victor V Kotlyar, *Procedia Eng*, 201(2017)169–176.
103. Kotlyar V V, Kovalev, A A, Porfirev A P, *Vortex Laser Beams*, (CRC Press Boca Raton FL, USA), 2019.
104. Kotlyar V V, Kovalev A A, Nalimov A G, *Topological Charge of Optical Vortices*, (CRC Press, Boca Raton FL, USA), 2023.
105. Senthilkumaran P, *Singularities in Physics and Engineering*, (IOP Publ. Bristol UK), 2018.
106. Gbur G G, *Singular Optics*, (CRC Press, Boca Raton FL, USA), 2017.
107. Rosales-Guzman C, Forbes A, *How to Shape Light with Spatial Light Modulators*, (SPIE Press Bellingham WA), 2017.
108. Vashisth S, Singh H, Yadav A K, Singh K, Devil's vortex phase structure as frequency plane mask for image encryption using the fractional Mellin transform, *Int J Opt*, 2014(2014)728056; /doi.org/10.1155/2014/728056.

109. Vashisth S, Singh H, Yadav A K, Singh K, Image encryption using fractional Mellin transform, structured phase filters, and phase retrieval, *Optik*, 125(2014)5309–5315.
110. Singh H, Yadav A K, Vashisth S, Singh K, Fully phase image encryption using double random-structured phase masks in gyrator domain, *Appl. Opt.*, 53(2014)6472–6481.
111. Singh H, Yadav A K, Vashisth S, Singh K, Double phase-image encryption using gyrator transforms, and structured phase mask in the frequency plane, *Opt Lasers Eng*, 67(2015)145–156.
112. Yadav A K, Vashisth, Singh H, Singh K, A phase-image watermarking scheme in gyrator domain using devil's vortex Fresnel lens as a phase mask *Opt. Commun* 344(2015)172–180.
113. Singh H, Yadav A K, Vashisth S, Singh K, Optical image encryption using devil's vortex toroidal lens in the Fresnel transform domain, *Int J Opt*, 2015(2015)926135; doi.org/10.1155/2015/926135.
114. Singh H, Yadav A K, Vashisth S, Singh K, A cryptosystem for watermarking based on fractional Fourier transform using a random phase mask in the input plane and a structured phase mask in the frequency plane, *Asian J Phys* 23(2014)597–612.
115. Singh H, Yadav A K, Vashisth S, Singh K, Double phase-image encryption using gyrator-,and fractional Fourier transforms with structured phase mask in the frequency plane followed by a gyrator transform, *Asian J Phys* 24(2015)1–16.
116. Kumar R, Sakshi, Singh K, An asymmetric optical cryptosystem based on Radon transform for phase image encryption, *Asian J Phys* 31(2022)A1–A12.
117. Yadav A K, Vashisth S, Singh H, Singh K, Optical cryptography and watermarking using some fractional canonical transforms and structured masks, in “*Adv Opt Sci Eng*” Proc IEM OPTRONIX 2014, Kolkata, Eds V. Lakshminarayanan and I. Bhattacharya, (Springer Proc Physics), Vol166, 2015, pp 25–36.
118. Yadav S, Singh H, Security augmentation grounded on Fresnel and Arnold transforms using hybrid chaotic structured phase mask, *IET Image Process*, 15(2020)1042–1052.
119. Anshula, Singh H, Security-enrichment of an asymmetric optical image encryption-based devil's vortex Fresnel lens phase mask and lower upper decomposition with partial pivoting in gyrator transform domain, *Opt Quant Electron*, 53(2021)204; doi.org/10.1007/s11082-021-02854-7.
120. Anshula, Singh H, Cryptanalysis for double-image encryption using the DTLM in frequency plane with QR-decomposition and gyrator transform, *Opt Rev*, 28(2021)596–610.
121. Chen H, Liu Z, Tanougast C, Blondel W, Asymmetric optical cryptosystem for multiple images based on devil's spiral Fresnel lens phase and random spiral transform in gyrator domain, *Sci Rep*, 11(2021)20846; doi.org/10.1038/s41598-021-00276-9.
122. Su Y, Wang X, Wang Z, Liu C, Li J, Xu K, Li S, Cai Z, Wan W, Security-enhanced multiple-image encryption based on modified phase retrieval algorithm with structured phase mask in Fresnel domain, *Optik*, 254(2022)168649; doi.org/10.1016/j.ijleo.2022.168649.
123. Yang Q, Xi Z, Zhang M, Ouyang X, Xu Y, Cao Y, Wang S, Zhu L, Li X, Ultra-secure optical encryption based on tightly focused perfect optical vortex beams, *Nanophoton*, 11(2022)1063–1070.
124. Zhang J, Yan A, Zhang H, Asymmetric encryption of invisible structured light 3D imaging, *Appl Sci (MDPI)*, 12(2022)3563; doi.org/10.3390/app12073563.
125. Mandapati V C, Vardhan H, Prabhakar S, Sakshi, Kumar R, Reddy S G, Singh R P, Singh K, Multi-user nonlinear optical cryptosystem based on polar decomposition and fractional vortex speckle patterns, *Photonics (MDPI)*, 10(2023)561; doi.org/10.3390/photonics10050561.

[Received: 15.07.2023; accepted: 30.07.2023]